

Fourier-Attentive Representation Learning: A Fourier-Guided Framework for Few-Shot Generalization in Vision-Language Models

Hieu Dinh Trung Pham Huy Minh Nhat Nguyen Cuong Tuan Nguyen
Vietnamese German University
Ho Chi Minh City, Vietnam

{104240027, 10423045}@student.vgu.edu.vn, cuong.nt2@vgu.edu.vn

Abstract

*Large-scale pre-trained Vision-Language Models (VLMs) have demonstrated strong few-shot learning capabilities. However, these methods typically learn holistic representations where an image’s domain-invariant structure is implicitly entangled with its domain-specific style. This presents an opportunity to further enhance generalization by disentangling these visual cues. In this paper, we propose **Fourier-Attentive Representation Learning (FARL)**, a novel framework that addresses this by explicitly disentangling visual representations using Fourier analysis. The core of our method is a dual cross-attention mechanism, where learnable representation tokens separately query an image’s structural features (from the phase spectrum) and stylistic features (from the amplitude spectrum). This process yields enriched, disentangled tokens that are then injected deep into the VLM encoders to guide adaptation. Our design, which includes an asymmetric injection strategy, forces the model to learn a more robust vision-language alignment. Extensive experiments on 15 datasets demonstrate the effectiveness of our approach.*

1. Introduction

Vision-Language Models (VLMs), such as CLIP[19], have revolutionized the field of computer vision by learning from vast amounts of image-text pairs on the Internet. A key strength of these models is their strong ability for zero-shot and few-shot transfer to downstream tasks through “prompting”, where natural language descriptions are used to describe classes. This paradigm shifts away from traditional supervised learning, which relies on fixed, discrete labels, towards a more flexible, open-vocabulary understanding of visual concepts.

To effectively adapt these foundation models for downstream tasks, recent research has focused on developing efficient fine-tuning strategies that avoid updating the en-

tire network. A well known line of work is prompt learning, pioneered in the vision domain by CoOp[33]. CoOp replaces hand-crafted text templates with a set of learnable, continuous vectors, or “prompts”, which are optimized on a few downstream examples. This core concept has been significantly advanced in subsequent works. This core concept has been significantly advanced by works that introduce instance-conditioning[32], multi-modal deep prompting[10], or adapter-style modules with shared representation spaces[29][26][5].

However, despite their success, a fundamental limitation persists across these methods: the learned prompts or representation tokens are “black-box” vectors. They entangle high-level semantic features, such as object shape and structure, with low-level, domain-specific statistics, such as texture, color, and lighting. This entanglement makes the model prone to overfitting on the superficial characteristics of the few training samples from base classes, consequently impairing its generalization ability to novel, unseen classes.

To address this feature entanglement and guide the model toward more generalizable representations, we turn to a fundamental principle in signal processing: the Fourier transform. It is a long-established property in vision science that the Fourier phase spectrum of an image preserves high-level semantics, such as object shape and structure, which are largely domain-invariant[15][16][18][25][27]. In contrast, the amplitude spectrum primarily captures lower-level statistics such as color, texture, and lighting, which are often domain-specific and vary between different environments. This natural decomposition offers a principled way of separate domain-agnostic structural cues from domain-specific stylistic cues.

In this paper, we propose Fourier-Attentive Representation Learning (FARL), a novel framework that leverages this Fourier-based insight to guide the learning of disentangled representations for VLM fine-tuning. Our method begins by decomposing each input image into its phase- and amplitude-only components. We then introduce a dual cross-attention mechanism where a set of learnable,

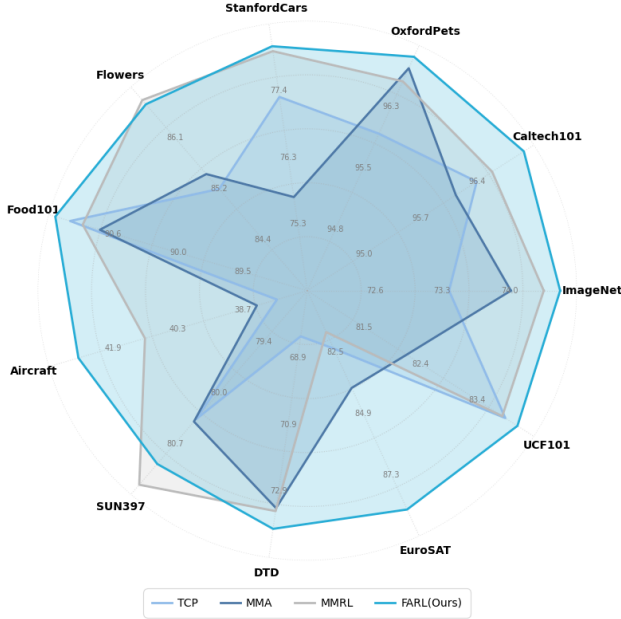


Figure 1. Comparison of the harmonic mean performance between the some previous method MMRL, MMA, TCP and our proposed FARL across 11 diverse datasets for base-to-novel generalization. modality-agnostic representation tokens are used to separately query the features extracted from the phase and amplitude streams. This process yields two specialized sets of tokens: structure-aware tokens informed by the phase information, and style-aware tokens informed by the amplitude information. These are then fused to create enriched, disentangled representation tokens. A key aspect of our design is an asymmetric injection strategy: the fused, feature-rich tokens are injected into the text encoder to form more descriptive and explicit internal prompts. In contrast, the image encoder is conditioned on the original, more general representation tokens. This forces the model to learn a more sophisticated alignment between a specific descriptive text representation and a general visual representation.

2. Related Work

2.1. Vision-Language Models

The development of Vision-Language Models (VLMs), pre-trained on massive web-scale datasets, has marked a significant milestone in artificial intelligence. Models like CLIP[19], ALIGN[9], and FILIP[30] earn a joint embedding space where visual and textual representations are aligned. This is typically achieved through a contrastive learning objective on hundreds of millions or even billions of image-text pairs. The primary strength of these models is their ability to perform zero-shot recognition, enabling them to generalize to a wide array of visual concepts without task-specific training. Our work builds upon this foundation, aiming to enhance the adaptability of these models

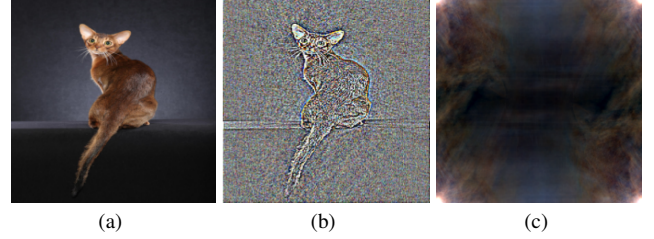


Figure 2. **Illustration of image reconstruction from the Phase and Amplitude of the Fourier transform.** (a) The original image. (b) The phase-only image, retains the high-level structural features. (c) The amplitude-only image, retains low-level stylistic features.

in few-shot scenarios.

2.2. Efficient Transfer Learning for VLMs

Adapting large VLMs to downstream tasks without incurring prohibitive computational costs or forgetting is a critical challenge. To this end, several efficient fine-tuning strategies have emerged. **Prompt Learning** methods, from the foundational CoOp[33] to more advanced variants like instance-conditional CoCoOp[32] and multi-modal MaPLe[10], have focused on optimizing input representations. Concurrently, **adapter-based approaches** such as MMA[26] and **representation learning frameworks** like MMRL[5] have explored deep-layer interactions. While these strategies have pushed performance boundaries, they fundamentally learn holistic representations, leaving the challenge of explicit feature disentanglement unaddressed.

2.3. Fourier Properties in Visual Representation

The core inspiration for our method stems from the well-established properties of the 2D Fourier transform in image analysis. For decades, it has been known that the phase and amplitude spectra of an image encode different kinds of information. The seminal work by Oppenheim et al.[15] demonstrated that Fourier phase is critical for preserving an image’s structural integrity; an image reconstructed using only its original phase and a constant magnitude retains a high degree of recognizability. More recent studies have formalized this observation[15][16][18][25][27], establishing that the phase spectrum contains high-level semantic information, such as object shapes and contours, which are robust to domain shifts. In contrast, the amplitude spectrum captures low-level statistics like color, texture, and lighting, which are often domain-specific. This principle has been successfully applied to tasks like domain generalization through data augmentation techniques that manipulate the amplitude spectrum while preserving the phase[25][27]. Inspired by this fundamental decomposition, our work directly guide the learning of disentangled and structured representations for VLM adaptation.

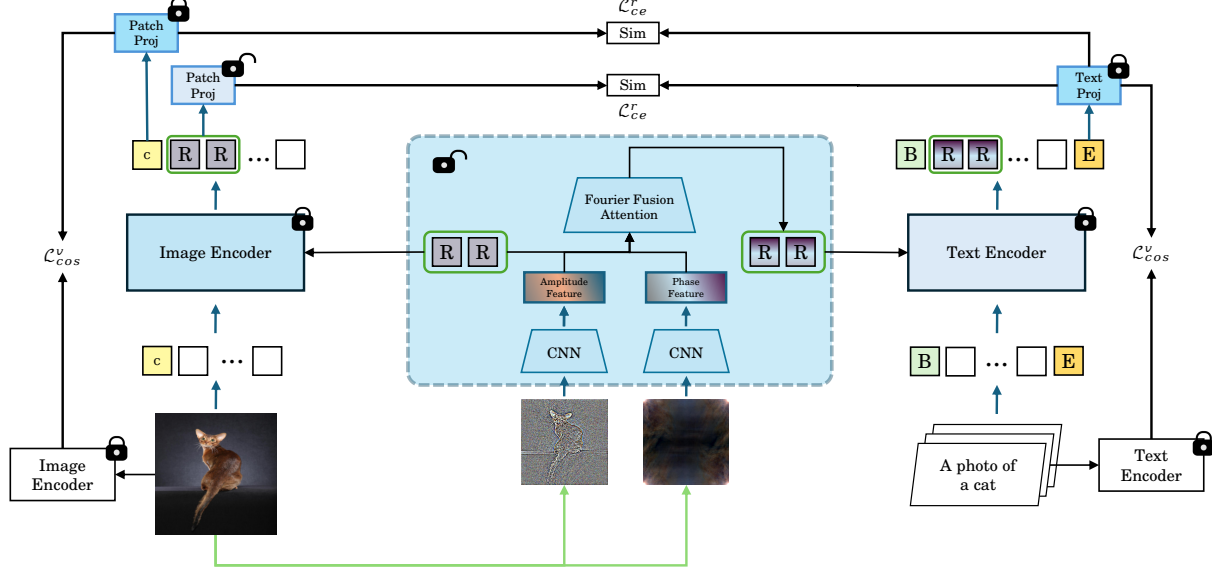


Figure 3. Overview of the FARL architecture. An image is decomposed into phase (structure) and amplitude (style) components. The Fourier Fusion Attention module (Fig. 4) uses these disentangled features to enrich learnable representation tokens R . Following an asymmetric injection strategy, the fused tokens are injected into the Text Encoder, while the original R tokens are injected into the Image Encoder. The model is optimized with a combination of cross-entropy \mathcal{L}_{ce} and cosine regularization \mathcal{L}_{cos} losses. Symbols: c : class token, B/E : text boundaries, R : representation tokens, F : projection layers.

3. Method

Our proposed framework, **Fourier-Attentive Representation Learning (FARL)**, introduces a novel adaptation strategy for Vision-Language Models (VLMs) that directly addresses the challenge of feature entanglement by operating in the Fourier domain. The framework is designed to learn disentangled, interpretable, and generalizable representations from few-shot data. The overall pipeline is illustrated in Fig. 3.

3.1. Preliminary: The CLIP Architecture

Image and Text Encoders: The CLIP Image Encoder \mathcal{V} , and Text Encoder \mathcal{T} , are typically based on the Transformer architecture. For an input image I , \mathcal{V} processes a sequence of patch embeddings E_0 prepended with a class token c_0 . This sequence is passed through L layers, and the final image feature f_v is projected from the output class token c_L . Similarly, \mathcal{T} processes a sequence of word embeddings W_0 framed by a Beginning-of-Text (b_0) and End-of-Text (e_0) token. This sequence is also passed through L layers, and the final text feature f_t is projected from the output EOT token e_L .

$$[c_i, E_i] = \mathcal{V}_i([c_{i-1}, E_{i-1}]), \quad 1 \leq i \leq L \quad (1)$$

$$[b_i, W_i, e_i] = \mathcal{T}_i([b_{i-1}, W_{i-1}, e_{i-1}]), \quad 1 \leq i \leq L \quad (2)$$

Zero-Shot Classification: CLIP performs zero-shot classification by computing the cosine similarity between

an image feature f_v and a set of text features $\{f_{t,c}\}_{c=1}^C$, generated from prompts for all C classes. The prediction probability is given by a softmax over these similarities, enabling classification without task-specific training.

3.2. FARL: A Fourier-Guided Approach

The core hypothesis of FARL is that by explicitly separating an image’s high-level, domain-invariant structure from its low-level, domain-specific style, we can guide a VLM to learn more robustly and avoid overfitting on superficial cues. Our framework achieves this through three key stages: (1) disentangling visual features via Fourier decomposition, (2) generating feature-rich representations using a dual-attention mechanism, and (3) asymmetrically adapting the VLM encoders with these representations.

3.2.1. Fourier Decomposition and Feature Extraction

The initial stage of FARL is to decompose an input image $I \in \mathbb{R}^{B \times C \times H \times W}$ into two distinct components that isolate its structural and stylistic information. This process begins by applying a 2D Fast Fourier Transform:

$$\mathcal{F}(I) = A \cdot e^{jP} \quad (3)$$

where $A = |\mathcal{F}(I)|$ and $P = \angle \mathcal{F}(I)$ are the amplitude and phase spectra, respectively. Using the inverse FFT \mathcal{F}^{-1} , we reconstruct two separate images:

Phase Image I_{phase} : To isolate structural information, the phase image is reconstructed by preserving the origi-

nal phase spectrum P while setting the amplitude spectrum to unity. This component retains high-level and domain-invariant features such as shapes and edges.

$$I_{\text{phase}} = \text{Re}(\mathcal{F}^{-1}(1 \cdot e^{jP})) \quad (4)$$

Amplitude Image I_{amp} : To isolate stylistic information, the amplitude image is reconstructed by preserving the original amplitude spectrum A while setting the phase spectrum to zero. This component captures low-level and domain-specific statistics such as color, texture, and lighting.

$$I_{\text{amp}} = \text{Re}(\mathcal{F}^{-1}(A \cdot e^{j \cdot 0})) \quad (5)$$

After independent normalization, these two component images are passed through lightweight CNNs to extract sequences of patch tokens, yielding a structure-focused feature set F_{phase} and a style-focused set F_{amp} .

These two images, after normalization, are passed through lightweight CNNs to produce sequences of patch tokens: a structure-focused feature set F_{phase} and a style-focused set F_{amp} .

3.2.2. Fourier-Attentive Representation Fusion

To leverage these disentangled features, FARL introduces a set of K learnable, modality-agnostic conceptual tokens, $R \in \mathcal{R}^{K \times D_{\text{rep}}}$. These tokens act as trainable queries to probe the two visual streams via a dual cross-attention mechanism, as shown in Fig. 3 and Fig. 4.

The mechanism generates two specialized sets of tokens: structure-aware R'_{phase} and style-aware R'_{amp} tokens:

$$R'_{\text{phase}} = \text{CrossAttn}_{\text{phase}}(Q = R; K, V = F_{\text{phase}}) \quad (6)$$

$$R'_{\text{amp}} = \text{CrossAttn}_{\text{amp}}(Q = R; K, V = F_{\text{amp}}) \quad (7)$$

These two sets are then fused by a fusion MLP $\mathcal{M}_{\text{fuse}}$ and integrated back into the original tokens via a weighted residual connection to produce the final, enriched representation tokens, R_{fused} .

$$R_{\text{fusion}} = \mathcal{M}_{\text{fuse}}(\text{Concat}(R'_{\text{phase}}, R'_{\text{amp}})) \quad (8)$$

$$R_{\text{fused}} = R + R_{\text{fusion}} \quad (9)$$

The resulting R_{fused} tokens now serve as a rich, disentangled semantic foundation for adapting the VLM.

3.2.3. Asymmetric Injection and Decoupled Inference

FARL employs an asymmetric adaptation strategy to inject the learned representations into the higher layers (from layer J onwards) of the VLM’s encoders.

Text Encoder: The enriched, fused tokens R_{fused} , which carry the disentangled structural and stylistic information, are projected and subsequently injected into the higher layers of the Text Encoder. For each target layer j

(where $J \leq j \leq L$), a dedicated projection function P_j^t maps the tokens:

$$R_j^t = \mathcal{P}_j^t(R_{\text{fused}}) \quad (10)$$

$$[b_j, R_j^t, W_j, e_j] = \mathcal{T}_j([b_{j-1}, R_{j-1}^t, W_{j-1}, e_{j-1}]) \quad (11)$$

The final text feature for a class c , $f_{t,c}$, is thus conditioned on the disentangled visual information, forming a richer, instance-specific representation.

Image Encoder: In contrast, the original, more general representation tokens R are projected and injected into the image encoder[5]. This process yields two distinct visual features: Class Feature f_v , derived from the original class token c path and Representation Feature f_r , derived from the injected representation tokens. For each target layer j (where $J \leq j \leq L$):

$$R_i^v = \mathcal{P}_i^v(R) \quad (12)$$

$$[c_i, R_i^v, E_i] = \mathcal{V}_i([c_{i-1}, R_{i-1}^v, E_{i-1}]) \quad (13)$$

Decoupled Learning Strategy: The two visual features, f_v and f_r , are leveraged differently for training and inference.

The training loss optimizes both features simultaneously, while a regularization term ensures the class feature path does not deviate significantly from the original CLIP space[5][19]:

$$\mathcal{L} = \alpha \mathcal{L}_{ce}(f_c) + (1 - \alpha) \mathcal{L}_{ce}(f_r) + \lambda(\mathcal{L}_{\text{cos}}^v + \mathcal{L}_{\text{cos}}^t) \quad (14)$$

A key strategy for robust generalization is the decoupled use of features during inference[5]:

- For **Base Classes** (seen during training): the final prediction combines the logits of both the class feature f_v and the representation feature f_r , leveraging both general and task-specific knowledge.
- For **Novel Classes** (unseen during training): the prediction relies only on the more general class feature f_c , which retains more of the pre-trained model’s robust, zero-shot capabilities.

4. Experiments

In this section, we conduct extensive experiments to evaluate the effectiveness of our proposed Fourier-Attentive Representation Learning (FARL) framework. We aim to answer the following key questions:

In this section, we conduct a series of experiments to comprehensively evaluate our proposed Fourier-Attentive Representation Learning (FARL) framework against state-of-the-art methods across four standard benchmarks. Our goal is to empirically validate FARL’s effectiveness in few-shot adaptation, generalization to unseen concepts, and robustness to distribution shifts. In-depth analysis and ablation studies are presented in Section 5.

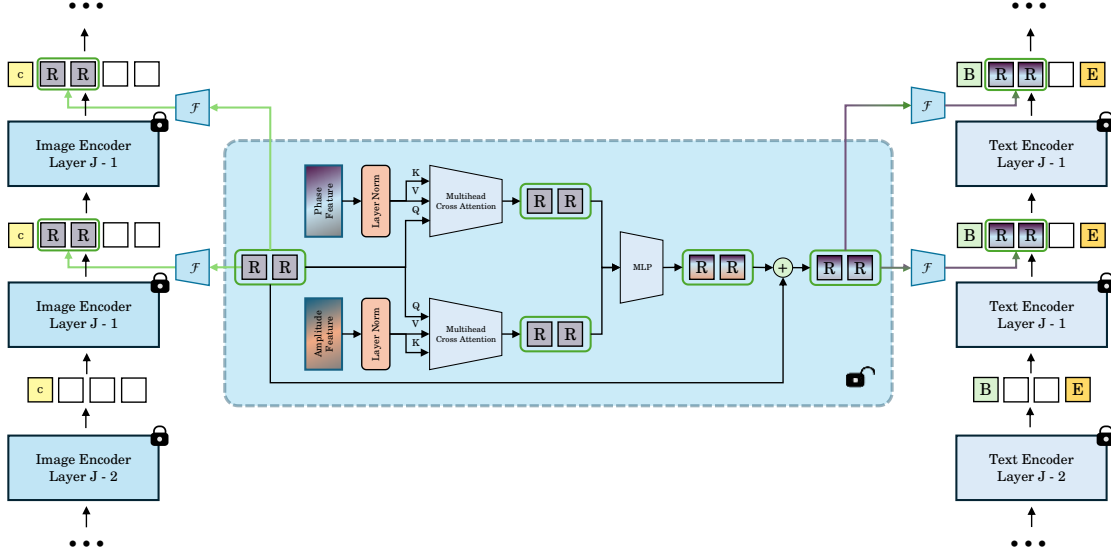


Figure 4. The Fourier Fusion Attention module. The module uses original representation tokens R as Queries to attend to Phase and Amplitude Features as Keys/Values in parallel cross-attention blocks. The result are fused by an MLP and combined with the original R via a residual connection to produce the final enriched tokens.

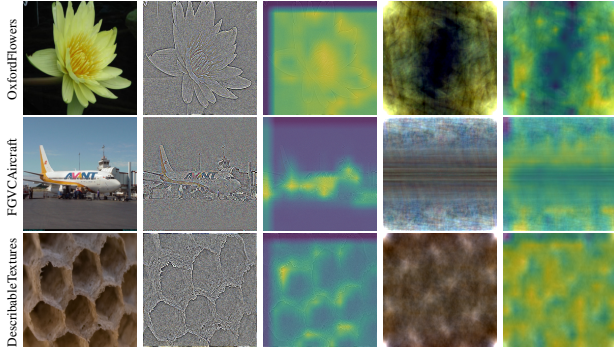


Figure 5. Visualization of Fourier decomposition and the dual-attention mechanism across diverse datasets. From left to right, each row displays: (1) the original image, (2) the phase-only reconstruction, (3) the attention map from the phase stream, (4) the amplitude-only reconstruction, and (5) the attention map from the amplitude stream.

4.1. Experimental Setup

Our evaluations are performed on a comprehensive suite of image classification datasets. For general-purpose tasks, we use 11 datasets: ImageNet[4], Caltech101[12], OxfordPets[17], Flowers102[14], Food101[1], FGVCAircraft[13], SUN397[23], DTD[3], EuroSAT[6], StanfordCars[11], and UCF101[21]. For the domain generalization task, we use ImageNet[4] as the source domain and evaluate on its four out-of-distribution variants: ImageNetV2[20], ImageNet-Sketch[22], ImageNet-A[8], and ImageNet-R[7].

We compare FARL against a range of strong and relevant baselines to position its performance, including: Zero-Shot CLIP[19], prompt learning methods such as CoOp[33], CoCoOp[32], KgCoOp[28], PLOT[2], ProVP[24], MetaPrompt[31], MaPLe[10], and TCP[29]; and other deep-layer adaptation methods such as MMA[26] and MMRL[5].

All models are built upon the ViT-B/16 CLIP backbone[19]. We primarily follow the 16-shot learning protocol, where 16 labeled examples per class are used for training. FARL are trained using the AdamW optimizer with an initial learning rate of 0.00005 and a cosine decay schedule, we set the number of representation tokens $K = 5$ and the injection start layer $J = 6$. All results are the average of three runs with different random seeds. For a fair comparison, results for MMRL were obtained by re-running the official source code under our experimental setup.

4.2. Base-to-Novel Generalization

This is our primary evaluation to assess the trade-off between learning on seen classes and generalizing to unseen ones. For each dataset, the classes are split into two disjoint sets: base and novel. The model is trained only on the Base classes and evaluated on both. We report the accuracy on Base classes (measuring few-shot learning performance), accuracy on Novel classes (measuring zero-shot generalization), and the Harmonic Mean (HM) of the two as a balanced metric. Tabl. 1.

| Datasets | Sets | CLIP (ICML2021) | CoOp (IJCV22) | CoCoOp (CVPR22) | KgCoOp (CVPR23) | PLOT (ICLR23) | MaPLe (CVPR23) | ProVP (IJCV2024) | MetaPrompt (TIP2024) | TCP (CVPR2024) | MMA (CVPR2024) | MMRL (CVPR2025) | FARL (our) |
|--------------|-------|--------------------|------------------|--------------------|--------------------|------------------|-------------------|---------------------|-------------------------|-------------------|-------------------|--------------------|---------------|
| Average | Base | 69.34 | 82.38 | 80.47 | 80.73 | 83.98 | 82.28 | 85.20 | 83.66 | 84.13 | 83.20 | 85.66 | 86.11 |
| | New | 74.22 | 67.96 | 71.69 | 73.61 | 71.72 | 75.14 | 73.23 | 75.48 | 75.36 | 76.94 | 76.19 | 77.49 |
| | HM | 71.59 | 73.89 | 75.44 | 76.71 | 76.76 | 78.27 | 78.38 | 79.08 | 79.26 | 79.72 | 80.65 | 81.57 |
| ImageNet | Base | 72.43 | 76.46 | 75.98 | 75.83 | 77.30 | 76.66 | 75.82 | 77.52 | 77.27 | 77.31 | 77.80 | 78.03 |
| | New | 68.14 | 66.31 | 70.43 | 69.96 | 69.87 | 70.54 | 69.21 | 70.83 | 69.87 | 71.23 | 71.13 | 71.33 |
| | HM | 70.22 | 71.02 | 73.10 | 72.78 | 73.40 | 73.47 | 72.36 | 74.02 | 73.38 | 74.02 | 74.37 | 74.53 |
| Caltech101 | Base | 96.84 | 97.80 | 97.96 | 97.72 | 98.53 | 97.74 | 98.92 | 98.13 | 98.23 | 98.40 | 98.83 | 99.23 |
| | New | 94.00 | 93.27 | 93.81 | 94.39 | 92.80 | 94.36 | 94.21 | 94.58 | 94.67 | 94.00 | 94.50 | 94.93 |
| | HM | 95.40 | 95.48 | 95.84 | 96.03 | 95.58 | 96.02 | 96.51 | 96.32 | 96.42 | 96.15 | 96.62 | 97.03 |
| OxfordPets | Base | 91.17 | 94.47 | 95.20 | 94.65 | 94.50 | 95.43 | 95.87 | 95.53 | 94.67 | 95.40 | 95.87 | 96.10 |
| | New | 97.26 | 96.00 | 97.69 | 97.76 | 96.83 | 97.76 | 97.65 | 97.00 | 97.20 | 98.07 | 97.27 | <i>97.63</i> |
| | HM | 94.12 | 95.23 | 96.43 | 96.18 | 95.65 | 96.58 | 96.75 | 96.26 | 95.92 | 96.72 | 96.56 | 96.86 |
| StanfordCars | Base | 63.37 | 75.67 | 70.49 | 71.76 | 79.07 | 72.94 | 80.43 | 76.34 | 80.80 | 78.50 | 81.50 | 81.43 |
| | Novel | 74.89 | 67.53 | 73.59 | 75.04 | 74.80 | 74.00 | 67.96 | 75.01 | 74.13 | 73.10 | 74.90 | 75.10 |
| | HM | 68.65 | 71.37 | 72.01 | 73.36 | 76.88 | 73.47 | 73.67 | 75.48 | 77.32 | 75.70 | 78.06 | 78.14 |
| Flowers | Base | 72.08 | 97.27 | 94.87 | 95.00 | 97.93 | 95.92 | 98.42 | 97.66 | 97.73 | 97.77 | 98.87 | 98.9 |
| | New | 77.80 | 67.13 | 71.75 | 74.73 | 73.53 | 72.46 | 72.06 | 74.49 | 75.57 | 75.93 | 77.23 | 77.1 |
| | HM | 74.83 | 79.44 | 81.71 | 83.65 | 83.99 | 82.56 | 83.20 | 84.52 | 85.23 | 85.48 | 86.72 | 86.65 |
| Food101 | Base | 90.10 | 89.37 | 90.70 | 90.5 | 89.80 | 90.71 | 90.32 | 90.74 | 90.57 | 90.13 | 90.33 | 90.67 |
| | New | 91.22 | 88.77 | 91.29 | 91.7 | 91.37 | 92.05 | 90.91 | 91.85 | 91.37 | 91.30 | 91.40 | <i>91.53</i> |
| | HM | 90.66 | 89.07 | 90.99 | 91.09 | 90.58 | 91.38 | 90.61 | 91.29 | 90.97 | 90.71 | 90.86 | <i>91.10</i> |
| Aircraft | Base | 27.19 | 39.67 | 33.41 | 36.21 | 42.13 | 37.44 | 47.08 | 40.14 | 41.97 | 40.57 | 45.97 | 49.57 |
| | New | 36.29 | 31.23 | 23.71 | 33.55 | 33.73 | 35.61 | 29.87 | 36.51 | 34.43 | 36.33 | 37.20 | 37.63 |
| | HM | 31.09 | 34.95 | 27.74 | 34.83 | 37.46 | 36.50 | 36.55 | 38.24 | 37.83 | 38.33 | 41.12 | 42.78 |
| SUN397 | Base | 69.36 | 80.85 | 79.74 | 80.29 | 82.20 | 80.82 | 80.67 | 82.26 | 82.63 | 82.27 | 83.23 | 83.00 |
| | New | 75.35 | 68.34 | 76.86 | 76.53 | 73.63 | 78.70 | 76.11 | 79.04 | 78.20 | 78.57 | 79.20 | 78.93 |
| | HM | 72.23 | 74.07 | 78.27 | 78.36 | 77.68 | 79.75 | 78.32 | 80.62 | 80.35 | 80.38 | 81.17 | 80.91 |
| DTD | Base | 53.24 | 79.97 | 77.01 | 77.55 | 81.97 | 80.36 | 83.95 | 83.10 | 82.77 | 83.20 | 85.63 | 85.03 |
| | New | 59.90 | 48.60 | 56.00 | 54.99 | 43.80 | 59.18 | 59.06 | 58.05 | 58.07 | 65.63 | 64.33 | <i>65.50</i> |
| | HM | 56.37 | 60.46 | 64.85 | 64.35 | 57.09 | 68.16 | 69.34 | 68.35 | 68.25 | 73.38 | 73.47 | 74.00 |
| EuroSAT | Base | 56.48 | 90.10 | 87.49 | 85.64 | 93.70 | 94.07 | 97.12 | 93.53 | 91.63 | 85.46 | 95.93 | <i>96.67</i> |
| | New | 64.05 | 53.00 | 60.04 | 64.34 | 62.67 | 73.23 | 72.91 | 75.21 | 74.73 | 82.34 | 71.10 | 82.73 |
| | HM | 60.03 | 66.74 | 71.21 | 73.48 | 75.11 | 82.30 | 83.29 | 83.38 | 82.32 | 83.87 | 81.67 | 88.66 |
| UCF101 | Base | 70.53 | 84.53 | 82.33 | 82.89 | 86.60 | 83.00 | 88.56 | 85.33 | 87.13 | 86.23 | 88.17 | <i>88.53</i> |
| | New | 77.50 | 67.37 | 73.45 | 76.67 | 75.90 | 78.66 | 75.55 | 77.72 | 80.77 | 80.03 | 79.80 | 79.97 |
| | HM | 73.85 | 74.98 | 77.67 | 79.65 | 80.90 | 80.77 | 81.54 | 81.35 | 83.83 | 82.20 | 83.78 | 84.03 |

Table 1. Comparison of FARL with previous methods on base-to-novel generalization across 10 datasets. **Bold** indicates the best performance among all compared methods. Results shown in *blue italics* outperform previous SOTA method MMRL.

4.3. Cross-Dataset Evaluation

To assess transferability, we train models on the 1000 classes of ImageNet and directly evaluate them on the other 10 datasets in a zero-shot manner. The results in Tabl. 2 indicate that FARL maintains strong performance across diverse and unseen datasets, achieving the highest average accuracy. This highlights the transferability of the disentangled representations learned by our method.

4.4. Domain Generalization

We evaluate the robustness of the ImageNet-trained models on datasets with significant domain shifts (e.g., photos to sketches). As presented in Tabl. 3, FARL demonstrates superior robustness to domain shifts compared to all baselines. We attribute this to the model’s reliance on domain-invariant structural features extracted from the Fourier phase.

5. Analysis and Ablation Studies

5.1. Qualitative Analysis: Visualizing Disentanglement

To provide an intuitive and visual validation of our core hypothesis, that FARL successfully learns to disentangle structural and stylistic features, we conduct a qualitative analysis of the attention maps generated by our dual cross-attention mechanism. By visualizing where the model “looks” within the phase and amplitude streams, we can gain insights into its decision-making process.

5.1.1. Case Study 1: Object Recognition

Phase Attention: The attention maps from the phase stream focus on the core structural elements of the subject. Across the different representation tokens, high-attention regions localize on the cat’s head, and the curvature of its back and tail. This provides strong evidence that the phase

| | Source | Target | | | | | | | | | | |
|----------------------|--------------|--------------|--------------|--------------|--------------|--------------|--------------|--------------|--------------|--------------|--------------|--------------|
| | ImageNet | Average | Caltech101 | OxfordPets | StanfordCars | Flowers101 | Food101 | FGVCAircraft | SUN397 | DTD | EuroSAT | UCF101 |
| CoOpOp (CVPR2022) | 71.02 | 65.74 | 94.43 | 90.14 | 65.32 | 71.88 | 86.06 | 22.94 | 67.36 | 45.73 | 45.37 | 68.21 |
| MaPLe (CVPR2023) | 70.72 | 66.30 | 93.53 | 90.49 | 65.57 | 72.23 | 86.20 | 24.74 | 67.01 | 46.49 | 48.06 | 68.69 |
| TCP (CVPR2024) | 71.40 | 66.29 | 93.97 | 91.25 | 64.69 | 71.21 | 86.69 | 23.45 | 67.15 | 44.35 | 51.45 | 68.73 |
| MMA (CVPR2024) | 71.00 | 66.61 | 93.80 | 90.30 | 66.13 | 72.07 | 86.12 | 25.33 | 68.17 | 46.57 | 49.24 | 68.32 |
| MMRL (CVPR2025) | 73.70 | 66.13 | 94.43 | 91.30 | 64.67 | 71.87 | 85.10 | 25.37 | 67.00 | 44.03 | 48.60 | 68.93 |
| FARL _{Ours} | 73.43 | 66.84 | 94.53 | 91.70 | <i>66.07</i> | 72.47 | <i>86.07</i> | 25.97 | <i>67.53</i> | <i>44.60</i> | <i>50.67</i> | 68.83 |

Table 2. Comparison of FARL with previous methods on cross-dataset evaluation across 10 datasets.

Table 3. Comparison of FARL with previous methods on domain generalization across 4 datasets.

| | Source | Target | | | |
|----------------------|--------------|--------------|--------------|--------------|--------------|
| | ImageNet | -V2 | -S | -A | -R |
| CLIP (ICML2021) | 66.73 | 60.83 | 46.15 | 47.77 | 73.96 |
| CoOpOp (CVPR2022) | 71.02 | 64.07 | 48.75 | 50.63 | 76.18 |
| MaPLe (CVPR2023) | 70.72 | 64.07 | 49.15 | 50.90 | 76.98 |
| MMA (CVPR2024) | 71.00 | 64.33 | 49.13 | 51.12 | 77.32 |
| MMRL (CVPR2025) | 73.70 | 65.43 | 48.70 | 50.13 | 76.63 |
| FARL _{Ours} | 73.43 | 64.83 | 49.23 | <i>50.57</i> | <i>77.20</i> |

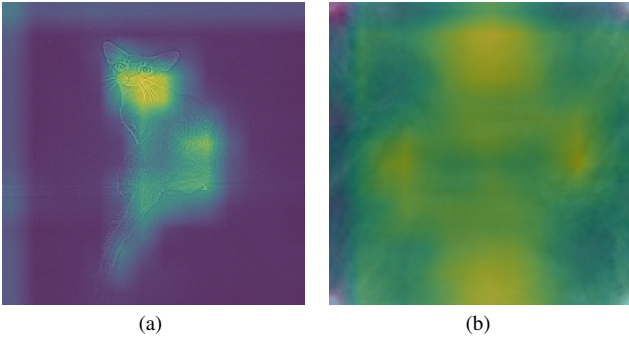


Figure 6. **Visualization of Attention from the Dual Fourier Streams.** (a) Attention from the phase stream. (b) Attention from the amplitude stream.

stream guides the model to identify what the object is by concentrating on its defining, domain-invariant shape.

Amplitude Attention: Conversely, the amplitude-attentive maps exhibit a more diffuse pattern. They concentrate on broader regions characterized by color and texture, such as the warm, orange-brown tones of the cat’s fur and the dark, uniform background. This suggests that the amplitude stream learns how the object appears in terms of its style, color, and surrounding lighting context.

5.1.2. Case Study 2: Scene Recognition

This disentanglement behavior is not only limited to object-centric images, as shown in Figure 7 for a satellite image of a ”Highway” from the EuroSAT dataset[6].

Phase Attention: Despite the noisy, almost texture-like appearance of the phase-only image, the phase-attentive



Figure 7. The original image, phase-only image, amplitude-only image, attention from the phase stream and attention from the amplitude stream.

maps successfully and highlight the key geometric features: the shape of the roads. The attention mechanism effectively filters the noise to isolate the domain-invariant structure that defines a ”highway”.

Amplitude Attention: In contrast, the amplitude-attentive maps show almost no focus on the sharp edges of the roads. Instead, they concentrate on the areas of color and texture, such as the green patches of grass and the gray asphalt. This shows a clear separation of concerns.

5.2. The Principle of Fourier-Guided Disentanglement

The effectiveness of our Fourier-based approach is rooted in the fundamental properties of the 2D Fourier transform, as established in previous works. The rationale is that phase and amplitude spectra encode distinct and complementary aspects of an image:

Phase Encodes Structure: The phase spectrum governs the spatial localization of frequency components. It acts as a blueprint, dictating the precise alignment required for constructive interference to form structural features like edges and contours. This information, representing the domain-invariant ”what” of an image, is critical for robust object recognition.

Amplitude Encodes Style: Conversely, the amplitude spectrum specifies the intensity of each frequency. Its distribution reflects global statistics such as color and contrast (low frequencies) and fine-grained textures (high frequencies). This makes amplitude the primary carrier of the domain-specific ”style” or ”how” an image appears.

Our FARL framework applies this principle through its dual cross-attention streams, which function as distinct ”experts”. The phase-attention module, acting as a structure detector, learns an object’s domain-invariant geometric properties from the phase-only image features. In contrast, the amplitude-attention module serves as a style sensor, captur-

ing domain-specific information like color and texture from the amplitude stream. By fusing these two streams, FARL creates a comprehensive representation that explicitly encodes both an object’s intrinsic structure and its extrinsic style.

The tangible benefit of this disentanglement is powerfully demonstrated by the model’s performance on the EuroSAT dataset. On this dataset, classes such as River or Highway are primarily defined by their geometric shapes. Conventional models, which process entangled features, can be “fooled” by stylistic cues from base classes (e.g., overfitting to “green texture” from vegetation classes). FARL mitigates this issue directly. Its phase-attention stream allows it to recognize novel classes based on their characteristic geometric structure, regardless of the surrounding terrain’s color. This ability to prioritize generalizable structural information is the direct reason for the significant +10.03% accuracy improvement on EuroSAT’s novel classes.

5.3. Ablation on Architectural Variants

To isolate the contributions of our key design choices, we evaluate several architectural variants of FARL: $FARL_{Phase}$, removed the amplitude stream to isolate the impact of structural features. $FARL_{Amplitude}$, removed the phase stream to test the efficacy of using only stylistic features. $FARL_{Spatial}$, replaced the Fourier decomposition with the original RGB image fed into both streams. And finally, $FARL_{Phase\&Spatial}$, replaced the amplitude stream with the original RGB image. This crucial baseline tests whether the performance gain stems from the dual-stream architecture itself or from the explicit Fourier-guided disentanglement.

Table 4. **Ablation study on architectural variants of FARL.** We report the average accuracy on Base and Novel classes, along with the Harmonic Mean (HM).

| Method | Base | Novel | HM |
|-------------------------|--------------|--------------|--------------|
| FARL | 86.11 | 77.49 | 81.57 |
| $FARL_{Phase}$ | 86.14 | 76.82 | 81.21 |
| $FARL_{Amplitude}$ | 83.86 | 73.05 | 78.08 |
| $FARL_{Spatial}$ | 86.09 | 76.88 | 81.22 |
| $FARL_{Phase\&Spatial}$ | 86.06 | 76.97 | 81.26 |

The results, averaged over 11 datasets in the 16-shot base-to-novel generalization setting, are summarized in Tabl. 4.

The $FARL_{Phase}$ variant retains strong performance, particularly on novel classes, confirming the primary role of domain-invariant structural information for generalization. However, the full FARL model performs best, indicating that stylistic cues from the amplitude stream offer valuable complementary information. In contrast, the $FARL_{Amplitude}$

variant shows a significant drop in performance, highlighting the risks of relying solely on domain-specific features.

Most importantly, the $FARL_{Spatial}$ and $FARL_{Phase\&Spatial}$ baseline, while performing competitively, underperforms the full FARL model. This result suggests that simply using a dual-stream architecture is not sufficient; the explicit disentanglement provided by the Fourier decomposition is the key contributor to our method’s enhanced generalization capabilities. These findings collectively validate the design of the FARL framework and the central role of its Fourier-guided mechanism.

6. Conclusion

In this work, we proposed FARL, a framework to address the challenge of feature entanglement in few-shot VLM adaptation. Our approach leverages the properties of the Fourier transform to disentangle an image’s structural and stylistic information. We introduced a dual cross-attention mechanism that allows learnable representation tokens to separately process these two feature streams, creating enriched representations that are then asymmetrically injected into the VLM’s encoders.

Experimental results on several benchmark datasets demonstrate the effectiveness of this approach. FARL shows notable improvements over strong baselines in base-to-novel generalization and domain generalization tasks. These findings suggest disentanglement via Fourier streams may help robustness and reduce reliance on stylistic cues. The principle of Fourier-guided feature disentanglement points toward potential directions for future work, and we believe that guiding representation learning with fundamental signal properties is a promising approach for building more generalizable VLM systems.

References

- [1] Lukas Bossard, Matthieu Guillaumin, and Luc Van Gool. Food-101 – mining discriminative components with random forests. pages 446–461, 2014. 5
- [2] Guangyi Chen, Weiran Yao, Xiangchen Song, Xinyue Li, Yongming Rao, and Kun Zhang. Plot: Prompt learning with optimal transport for vision-language models, 2023. 5
- [3] Mircea Cimpoi, Subhransu Maji, Iasonas Kokkinos, Sammy Mohamed, and Andrea Vedaldi. Describing textures in the wild, 2013. 5
- [4] Jia Deng, Wei Dong, Richard Socher, Li-Jia Li, Kai Li, and Li Fei-Fei. Imagenet: A large-scale hierarchical image database. In *2009 IEEE Conference on Computer Vision and Pattern Recognition*, pages 248–255, 2009. 5
- [5] Yuncheng Guo and Xiaodong Gu. Mmrl: Multi-modal representation learning for vision-language models, 2025. 1, 2, 4, 5
- [6] Patrick Helber, Benjamin Bischke, Andreas Dengel, and Damian Borth. Eurosat: A novel dataset and deep learning

- benchmark for land use and land cover classification, 2019. 5, 7
- [7] Dan Hendrycks, Steven Basart, Norman Mu, Saurav Kadavath, Frank Wang, Evan Dorundo, Rahul Desai, Tyler Zhu, Samyak Parajuli, Mike Guo, Dawn Song, Jacob Steinhardt, and Justin Gilmer. The many faces of robustness: A critical analysis of out-of-distribution generalization, 2021. 5
 - [8] Dan Hendrycks, Kevin Zhao, Steven Basart, Jacob Steinhardt, and Dawn Song. Natural adversarial examples, 2021. 5
 - [9] Chao Jia, Yinfei Yang, Ye Xia, Yi-Ting Chen, Zarana Parekh, Hieu Pham, Quoc Le, Yun-Hsuan Sung, Zhen Li, and Tom Duerig. Scaling up visual and vision-language representation learning with noisy text supervision. In *Proceedings of the 38th International Conference on Machine Learning*, pages 4904–4916. PMLR, 2021. 2
 - [10] Muhammad Uzair Khattak, Hanoona Rasheed, Muhammad Maaz, Salman Khan, and Fahad Shahbaz Khan. Maple: Multi-modal prompt learning, 2023. 1, 2, 5
 - [11] Jonathan Krause, Michael Stark, Jia Deng, and Li Fei-Fei. 3d object representations for fine-grained categorization. 2013. 5
 - [12] Fei Li, Rob Fergus, Pietro Perona, and Djabeur Zekrifa. Learning generative visual models from few training examples: An incremental bayesian approach tested on 101 object categories. *Computer Vision and Image Understanding*, 2013. 5
 - [13] Subhransu Maji, Esa Rahtu, Juho Kannala, Matthew Blaschko, and Andrea Vedaldi. Fine-grained visual classification of aircraft, 2013. 5
 - [14] Maria-Elena Nilsback and Andrew Zisserman. Automated flower classification over a large number of classes. In *Proceedings of the 2008 Sixth Indian Conference on Computer Vision, Graphics & Image Processing*, page 722–729, USA, 2008. IEEE Computer Society. 5
 - [15] A.V. Oppenheim, Jae Lim, Gary Kopec, and Stephen Pohlig. Phase in speech and pictures. pages 632 – 637, 1979. 1, 2
 - [16] Alan V. Oppenheim and Jae Sung Lim. The importance of phase in signals. *Proceedings of the IEEE*, 69:529–541, 1980. 1, 2
 - [17] Omkar M Parkhi, Andrea Vedaldi, Andrew Zisserman, and C. V. Jawahar. Cats and dogs. In *2012 IEEE Conference on Computer Vision and Pattern Recognition*, pages 3498–3505, 2012. 5
 - [18] Leon N. Piotrowski and Fergus W. Campbell. A demonstration of the visual importance and flexibility of spatial-frequency amplitude and phase. 11(3):337–346. eprint: <https://doi.org/10.1068/p110337>. 1, 2
 - [19] Alec Radford, Jong Wook Kim, Chris Hallacy, Aditya Ramesh, Gabriel Goh, Sandhini Agarwal, Girish Sastry, Amanda Askell, Pamela Mishkin, Jack Clark, Gretchen Krueger, and Ilya Sutskever. Learning transferable visual models from natural language supervision, 2021. 1, 2, 4, 5
 - [20] Benjamin Recht, Rebecca Roelofs, Ludwig Schmidt, and Vaishaal Shankar. Do imagenet classifiers generalize to imagenet?, 2019. 5
 - [21] Khurram Soomro, Amir Roshan Zamir, and Mubarak Shah. Ucf101: A dataset of 101 human actions classes from videos in the wild, 2012. 5
 - [22] Haohan Wang, Songwei Ge, Eric P. Xing, and Zachary C. Lipton. Learning robust global representations by penalizing local predictive power, 2019. 5
 - [23] Jianxiong Xiao, Krista A. Ehinger, James Hays, Antonio Torralba, and Aude Oliva. Sun database: Exploring a large collection of scene categories. *Int. J. Comput. Vision*, 119(1):3–22, 2016. 5
 - [24] Chen Xu, Yuhan Zhu, Haocheng Shen, Boheng Chen, Yixuan Liao, Xiaoxin Chen, and Limin Wang. Progressive visual prompt learning with contrastive feature re-formation, 2024. 5
 - [25] Qinwei Xu, Ruipeng Zhang, Ya Zhang, Yanfeng Wang, and Qi Tian. A fourier-based framework for domain generalization. 1, 2
 - [26] Lingxiao Yang, Ru-Yuan Zhang, Yanchen Wang, and Xiaohua Xie. MMA: Multi-modal adapter for vision-language models. In *2024 IEEE/CVF Conference on Computer Vision and Pattern Recognition (CVPR)*, pages 23826–23837. IEEE. 1, 2, 5
 - [27] Yanchao Yang and Stefano Soatto. Fda: Fourier domain adaptation for semantic segmentation, 2020. 1, 2
 - [28] Hantao Yao, Rui Zhang, and Changsheng Xu. Visual-language prompt tuning with knowledge-guided context optimization, 2023. 5
 - [29] Hantao Yao, Rui Zhang, and Changsheng Xu. Tcp:textual-based class-aware prompt tuning for visual-language model, 2024. 1, 5
 - [30] Lewei Yao, Runhui Huang, Lu Hou, Guansong Lu, Minzhe Niu, Hang Xu, Xiaodan Liang, Zhenguo Li, Xin Jiang, and Chunjing Xu. Filip: Fine-grained interactive language-image pre-training, 2021. 2
 - [31] Cairong Zhao, Yubin Wang, Xinyang Jiang, Yifei Shen, Kaitao Song, Dongsheng Li, and Duoqian Miao. Learning domain invariant prompt for vision-language models, 2023. 5
 - [32] Kaiyang Zhou, Jingkang Yang, Chen Change Loy, and Ziwei Liu. Conditional prompt learning for vision-language models, 2022. 1, 2, 5
 - [33] Kaiyang Zhou, Jingkang Yang, Chen Change Loy, and Ziwei Liu. Learning to prompt for vision-language models. *International Journal of Computer Vision*, 130(9):2337–2348, 2022. 1, 2, 5